Preparation, structure, and spectroscopic properties of Nd³⁺:{La₁₋ₓLuₓ}₃[Lu₁₋ᵧGaᵧ]₂Ga₃O₁₂ crystals

Toomas H. Allik and Susan A. Stewart

Science Applications International Corporation, 1710 Goodridge Drive, P.O. Box 1303, McLean, Virginia 22102

Dhiraj K. Sardar,* Gregory J. Quarles, and Richard C. Powell

Department of Physics, Oklahoma State University, Stillwater, Oklahoma 74078-0444

Clyde A. Morrison and Gregory A. Turner

Harry Diamond Laboratories, U.S. Army Laboratory Command (LABCOM), Adelphi, Maryland 20783-1197

Milan R. Kokta

Union Carbide Corporation, 750 South 32nd Street, P.O. Box 6381, Washougal, Washington 98671

Wayne W. Hovis and Albert A. Pinto

Center for Night Vision & Electro-Optics, U.S. Army Electronics Research and Development Command (ERDCOM), Fort Belvoir, Virginia 22060-5567

Single crystals of lanthanum lutetium gallium garnet (LaLuGaG) were grown by the Czochralski pulling technique. X-ray diffraction and elemental analysis performed on these samples indicate that these garnets do not form with simple stoichiometry described as {La}₃[Lu]₂Ga₃O₁₂ but with increased Lu concentration in the dodecahedral site and Ga occupancy in the octahedral site. Optical absorption and fluorescence spectra confirm these results, showing inhomogeneous broadening of the spectral lines of Nd³⁺. Various laser gain measurements were performed on {La₁₋ₓLuₓ}₃[Lu₁₋ᵧGaᵧ]₂Ga₃O₁₂ crystals containing 4.3 and 1.3 at. % Nd³⁺ to determine the usefulness of this material as a laser. No optical gain was observed. Time-resolved, site-selection spectroscopy measurements were performed to determine the effects of ion-ion interaction, and show the presence of very weak energy transfer between ions in nonequivalent crystal-field sites. Two-photon excitation spectroscopy measurements demonstrate the presence of very strong two-photon−absorption transitions, which prevents lasing in this garnet.

I. INTRODUCTION

Although Nd-doped $Y_3Al_2(AlO_4)_3$ (YAG) has become a standard laser material, there is still significant interest in characterizing the properties of other types of Nd-doped materials that can be pumped with $Ga_{2-x}Al_xAs$ laser diodes emitting radiation at 800±20 nm. The spectral emission of laser diodes at 800 nm is resonant with the $^4F_{5/2}$ and $^2H_{9/2}$ Nd³⁺ absorption bands. The advantage derived from the spectral match leads to a reduction of the amount of heat which is deposited in the medium, thus reducing the thermomechanical requirements of the laser host. With the commercial availability of single laser diodes with powers exceeding 1 W and two-dimensional arrays producing 4.0 kW/cm², it is useful to determine if other materials can be found with spectral and thermo-optic properties leading to improved laser characteristics. Desirable properties of new laser-diode-pumped solid-state lasers include a longer fluorescence lifetime, a broader absorption band, and a higher absorption coefficient as compared to Nd:YAG. We report here the results of x-ray diffraction, elemental and spectroscopic analysis, and gain measurements obtained on Nd³⁺-doped {La₁₋ₓLuₓ}₃[Lu₁₋ᵧGaᵧ]₂Ga₃O₁₂ (LaLu-GaG) crystals.

$Y_3Al_2(AlO_4)_3$ is not the ideal garnet structure for doping with Nd³⁺ ions. The ionic radius of Nd³⁺ is too large to give polyhedra sides that match the sides of Al³⁺ polyhedra. This mismatch imposes difficulties in forming a solid solution of $Nd_3Al_2(AlO_4)_3$ with $Y_3Al_2(AlO_4)_3$ that would limit the amount of Nd³⁺ that can be incorporated into the YAG lattice to only a few atomic percent. In addition, the distances between cation lattice positions for the aluminum garnets are small enough to allow for strong enough ion-ion interaction to produce concentration quenching of the Nd³⁺ fluorescence.[1] On the other hand, neodymium may be substituted completely into gallium-based garnet systems. The largest lattice parameters in the gallium garnet group may be realized in garnets formed with lanthanum occupying the dodecahedral positions. For such garnets to be synthesized, the structure must be expanded by substitution of ions larger than gallium into the dodecahedral sites. When such substitutions were made, it was found[2] that compounds do not form with simple stoichiometry described as {La}₃[Lu]₂Ga₃O₁₂, but that the octahedral and tetrahedral substituents are distributed between two crystallographic sites, with the distribution corresponding to

the formula $\{La_{1-x}Lu_x\}_3[Lu_{1-y}Ga_y]_2Ga_3O_{12}$.

The study of mixed garnet crystals began in the late 1960s. Mixed garnets are those in which additional additives have been introduced into the $\{A\}_3[B]_2(C)_3O_{12}$ garnet crystal, causing multiple ions to occupy crystallographic sites. Numerous laboratories have studied the optical spectroscopy of mixed garnets, in particular Lu-compensated $Nd:Y_3Al_2(AlO_4)_3$. Holton *et al.*[3] showed inhomogeneous broadening of the spectral lines of Nd^{3+}, attributed to a distribution of Nd ions among sites with different crystalline fields. The resulting broadening is attributed to Nd ions residing in Lu-rich and Y-rich sites with slightly different crystal fields. Voron'ko and Sobol',[4] in a more comprehensive study of this mixed garnet system, investigated the dependence of the width and intensity of the spectral lines with respect to varying concentrations of Y and Lu in the dodecahedral sites. A slight broadening, by 2–10 times, was seen in these garnets, with no change of the intensities.

Doped with Nd, these mixed garnets are intermediate-gain laser materials, exhibiting gain higher than Nd:glass but lower than Nd:YAG. These materials would exhibit higher energy storage and lower amplified spontaneous emission at high pump powers.[5]

II. EXPERIMENTAL RESULTS

A. Crystal growth

The lanthanum lutetium gallium garnets of the above composition were grown by the standard Czochralski pulling technique. The raw materials were dried at 200 °C, and La_2O_3 and Lu_2O_3 were fired at 1100 °C for 12 h so that they would be free of absorbed water and carbon dioxide. The oxide was then mixed in the desired ratio, pressed in an isostatic press, and loaded into a 5×5 cm iridium crucible. rf power at a 9.8-kHz frequency was coupled via copper coil to the crucible, heating the crucible and melting the charge. The crucible was insulated with a stabilized zirconia sleeve, and the entire assembly (coil, insulation, and crucible) was enclosed in a water-cooled bell jar equipped with nitrogen and oxygen supply lines, providing a growth atmosphere of N_2 with 1 vol. % of O_2. The pulling rates employed were 1 mm/h. The fluid flow in the melt was aided by rotating of the crystal at the rate of 15 rpm. The crystal diameter was controlled at a programmed rate by regulating the weight of the growing crystal. The crystal grown in the [111] direction displayed typical garnet morphology, that is, faceting and core formation due to growth with a convex interface. The crystals were 1 in. in diameter and between 2 and 4 in. long. Numerous growth runs of these LaLuGaG crystals were performed with either or both Cr^{3+} and Nd^{3+}. The samples studied were two Nd-doped boules with 3.3 and 1.0 at. % added to the melt and one sample with 0.4 at. % Cr^{3+}. Spectroscopic samples of high optical quality were cut and polished from these boules.

B. X-ray diffraction

The spectroscopic characteristics of optically active ions in garnet crystals are closely related to the properties of the crystal structure. Originally determined by Menser[6] for naturally occurring minerals such as grossularite, spessartine, or pyrope, the garnet structure is cubic and belongs to space group $Ia\overline{3}d$. All the cations are in special positions with no degree of freedom, while the oxygen atoms are in general positions. Each oxygen atom is at a shared corner of four polyhedra: one tetrahedron surrounding a "d" ion; one octahedron surrounding an "a" ion; two dodecahedra surrounding "c" ions.

The positions of the oxygen ions in the structure are defined by three general parameters: x, y, and z. The values of these parameters change with the chemical composition of the garnets and depend mainly on the radii of the cations. When oxygen ions are shifted from their ideal positions, distortions of polyhedra result. These distortions change the length of the edges of the polyhedron, while the distances between the center and the corners of the polyhedron are given by cation-oxygen ionic radii. Thus, freedom in substitution of various cations in the garnet structure is greatly restricted by the requirement of matching the length of the shared edges among the three polyhedron types. On the other hand, expanding one polyhedron by proper selection of substituting cations may allow extending the selection of other cations for substituting into the garnet structure. This approach has been successful in doped lanthanum garnets.[2]

The crystal structure analysis was performed on an automated Nicolet R3m/μ diffractometer equipped with an incident-beam graphite monochromator and Mo $K\alpha$ radiation ($\lambda = 0.7107$ Å). Lattice parameters were determined for 2θ centered reflections within $3.0° < 2\theta < 60.0°$. Data were corrected for Lorentz-polarization effects and absorption correction. The structure of $\{La_{1-x}Lu_x\}_3[Lu_{1-y}Ga_y]_2Ga_3O_{12}$ was solved by direct methods by varying x and y until the R factors (or residuals) were minimized.[7] Low R factors indicate that the structure is correct and that the structure model based on atomic positions agrees well with the experimentally measured intensities. Table I shows the essential details of the structure; detailed structure information can be found in Ref. 8.

C. X-ray fluorescence

Elemental analysis was performed on three samples of LaLuGaG doped with impurities. These included two spectroscopic samples doped with Nd^{3+} and Cr^{3+}. The third sample was a 10-cm-long by 3-cm-diameter Nd^{3+}:LaLuGaG boule. The analysis was performed with a Kevex 770/8000 x-ray fluorescence spectrophotometer. This instrument uses the energy dispersive technique, where radiation from a primary x-ray tube is directed upon a secondary target, generating monochromatic x-ray fluorescent radiation at the characteristic $K\alpha$ and $K\beta$ energy levels of the target material. This secondary radiation is then directed upon the sample to be analyzed. The subsequent x-ray fluorescence from the sample is

TABLE I. Summary of single-crystal x-ray diffraction results of $\{La_{1-x}Lu_x\}_3[Lu_{1-y}Ga_y]_2Ga_3O_{12}$ for $x=0.25$ and $y=0$. Atom coordinates ($\times 10^4$) and thermal coefficients ($\text{Å}^2 \times 10^3$) of LaLuGaG. Space Group: $Ia\overline{3}d$ (cubic) (No. 230). Unit cell axis length: 12.930(3) Å. Observed data $[I \geq 3\sigma(I)]$: 236. Refinement: $R=4.07\%$; $wR=3.02\%$.

Atom	$10^4 x$	$10^4 y$	$10^4 z$	U (10^{-3} Å^2)
Lu(1)	0	0	0	21(1)[a]
La(2)	0	2500	1250	20(1)[a]
Lu(2)	0	2500	1250	20(1)[a]
Ga(3)	0	2500	3750	22(1)[a]
O	300(3)	576(3)	6569(3)	23(1)[a]

[a]Equivalent isotropic U defined as one third of the trace of the orthogonalized U_{ij} tensor. Parenthetical values are estimated standard deviations.

detected and recorded on a multichannel analyzer. The chief advantage of the energy dispersive system is that secondary targets can be chosen whose secondary x-ray fluorescence will most efficiently excite the analytes in question. Such efficient monochromatic excitation results in a high signal to background ratio and provides the ideal conditions for accurate quantification routines.

Film standards of known concentration and mass thickness were obtained from Micromatter Co.[9] to obtain a known intensity-concentration ratio. This known ratio is compared with the sample fluorescence intensities and is used in conjunction with excitation efficiencies and matrix effects to calculate analyte concentrations and the elemental composition of the sample.

In our analysis of these samples, we selected secondary targets which would most efficiently excite the analytes of interest with minimum peak overlapping. Other parameters such as tube voltage and current, counting time, and atmosphere were selected to provide a statistically valid number of counts and reduce atmospheric effects. The composition of three LaLuGaG single crystals is shown in Table II. The results in Table II clearly indicate the added presence of lutetium in positions other than that of the octahedral site. Based on size constraints, Lu undoubtedly occupies the dodecahedral site. These results were confirmed by x-ray diffraction. In addition, the Ga concentration was found to be slightly larger than three formula units, which would indicate occupancy in the octahedral site.

The segregation constant, k, for Nd^{3+}:LaLuGaG can be determined from the data in Table II. At equilibrium,

the concentration in the solid is given by[10]

$$c_s = kc_0(1-g)^{k-1},\qquad (1)$$

where c_0 is the initial concentration of the dopant ion and g is the fraction of melt that has been crystallized. For Nd^{3+} in LaLuGaG, k is 1.3.

D. Index of refraction

The refractive indices of Nd:LaLuGaG were measured using the method of minimum deviation,[11] in which a polished prism of Nd^{3+}:LaLuGaG was fabricated and mounted on a goniometer, and monochromatic light (in this case, from multiline argon ion and helium neon lasers) was passed through it. The point of least deflection is recorded as the angle of minimum deviation, and the index of refraction is calculated according to the formula

$$n = \sin[(\tfrac{1}{2})(\alpha+\eta_m)]/\sin(\tfrac{1}{2}\alpha),\qquad (2)$$

where α is the prism angle and η_m is the angle of minimum deviation. The results appear in Table III.

The accuracy of the refractive index calculated from the data was limited by the accuracy with which the angle of minimum deviation was measured, in this case 5″ of arc. Thus there existed an inherent error of ± 0.0025. The actual average error was ± 0.0035.

These experimental data were subsequently fit to Sellmeier's dispersion equation

$$n^2(\lambda) = 1 + S\lambda^2/(\lambda^2 - \lambda_0^2).\qquad (3)$$

TABLE II. LaLuGaG crystal composition in formula units.

Sample	Chemical analysis	Nd^{3+} concentration in LaLuGaG composition (at. %)	
		Crystal	Melt
Nd:LaLuGaG boule (top)	$Nd_{0.04}La_{2.32}Lu_{2.57}Ga_{3.07}O_{12.00}$	1.37±0.05	1.0
Nd:LaLuGaG boule (bottom)	$Nd_{0.04}La_{2.26}Lu_{2.63}Ga_{3.07}O_{12.00}$	1.30±0.05	1.0
Spectroscopic sample Nd:LaLuGaG	$Nd_{0.13}La_{2.14}Lu_{2.53}Ga_{3.20}O_{12.00}$	4.31±0.17	3.3
Spectroscopic sample Cr:LaLuGaG	$Cr_{0.4}La_{2.32}Lu_{2.61}Ga_{3.07}O_{12.00}$		

TABLE III. Indices of refraction of Nd^{3+}:LaLuGaG. Sellmeier coefficients: $n^2(\lambda) = 1 + S\lambda^2/(\lambda^2 - \lambda_0^2)$; $S = 2.3891$; $\lambda_0 = 194.46$ nm.

Wavelength (nm)	$n_{experimental}$
632.8	1.9070
611.9	1.9174
594.1	1.9221
543.0	1.9304
514.5	1.9376
496.5	1.9537
488.0	1.9632
476.5	1.9665

Appropriate values of S and λ_0, given in Table III, were calculated from this formula by averaging all the possible values extracted from the data. The index of refraction of maximum fluorescence in the $^4F_{3/2}$-$^4I_{11/2}$ transition, 1059 nm, was found to be 1.8634.
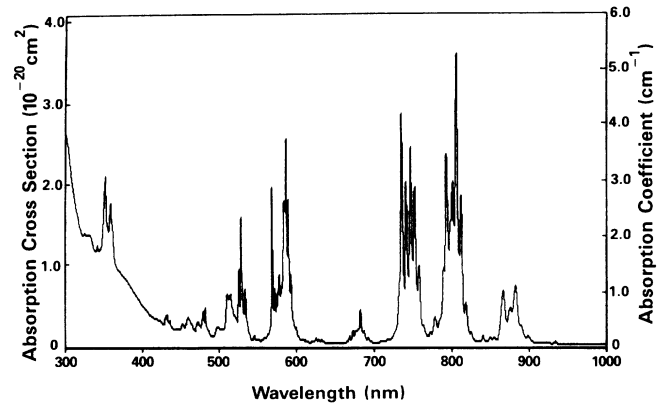

FIG. 1. Room-temperature absorption spectrum of Nd^{3+}:LaLuGaG (1.3 at. % Nd^{3+}). The sample thickness is 6.61 mm.

E. Nd^{3+} absorption spectra

The absorption spectrum of neodymium-doped LaLuGaG was investigated in the range of 200–6000 nm at room temperature and 10 K. These data were recorded

TABLE IV. Experimental (E) and theoretical (T) (the crystal-field parameters given in Table IX were used in the calculation of the energy levels) crystal-field splittings of Nd^{3+} ion manifolds in LaLuGaG.

State[a]		Stark-level positions (cm^{-1})
$^4I_{9/2}$	E	0, 102, 187, 287, 710
313	T	−6, 103, 191, 287, 711
$^4I_{11/2}$	E	1962, 2003, 2097, 2129, 2347, 2416
2177	T	1964, 2001, 2097, 2123, 2343, 2422
$^4I_{13/2}$	E	3899, 3920, 4040, 4059, 4315, 4338, 4407
4148	T	3901, 3915, 4039, 4051, 4317, 4337, 4412
$^4I_{15/2}$	E	5783, 5818, 5959, 6009, 6450, 6481, 6526, 6603
6190	T	5784, 5824, 5963, 6006, 6454, 6473, 6525, 6588
$^4F_{3/2}$	E	11417, 11534
11517	T	11414, 11531
$^2H_{9/2}$	E	12402, 12477, 12567, 12598, 12625, 12659,
$^4F_{5/2}$		12817, 12850
12383	T^b	12192, 12268, 12314, 12452, 12478, 12581,
12652		12622, 12656
$^4F_{7/2}$	E	13375, 13462, 13582, 13587,
$^4S_{3/2}$		13602, 13648
13501	T	13368, 13452, 13564, 13586,
13592		13597, 13659
$^4F_{9/2}$	E	14645, 14717, 14775, 14852, 14964
14770	T	14652, 14723, 14771, 14834, 14952
$^2H_{11/2}$	E	15901, 15926, 15991, 16093, 16129
15969	T^b	15908, 15939, 15961, 15968, 16011, 16054,
$^4G_{5/2}$	E	16951, 17042, 17116, 17324, 17586
$^2G_{7/2}$		
17091	T	16963, 17043, 17104, 17367,
17353		17434, 17465, 17653
$^2G_{9/2}$	E	18825, 18917, 18935, 19032, 19361, 19410,
$^4G_{7/2}$		19469, 19599, 19650
$^2P_{1/2}$	E	23217

[a]The multiplet in Russell-Saunders notation and centroids of that multiplet are given.
[b]Experimental energy levels not used in the crystal-field calculations. The aqueous centroids were used instead.

in the ultraviolet, visible, and near infrared on a Perkin-Elmer Lambda 9 spectrophotometer with a maximum resolution of 0.01 nm. A Perkin-Elmer 983G infrared spectrophotometer having an accuracy of 0.1 cm^{-1} was used to obtain spectra beyond 3200 nm.

A closed-cycle refrigerator, CTI-Cryogenics Model 21, was used to obtain spectra at 10 K. Sample temperatures were measured with a silicon diode calibrated to <1 K below 50 K. Typical cooldown times were 1 h.

Figure 1 shows the absorption spectrum at room temperature of Nd^{3+}:LaLuGaG between 300 and 1000 nm for a 0.661-cm-thick sample with a Nd^{3+} concentration of 1.45×10^{20} ions/cm^3. This spectrum is very typical of Nd^{3+} in other crystalline hosts, showing strong transitions from the $^4I_{9/2}$ ground-state multiplet to the $^2H_{9/2}$ and $^4F_{5/2}$ (800 nm), $^4F_{7/2}$ and $^4S_{3/2}$ (750 nm), and $^4G_{5/2}$ and $^2G_{7/2}$ (590 nm) states. The experimentally determined Stark levels of the Nd^{3+} ions in the dodecahedral sites are listed in Table IV.

The peak absorption (emission) cross section for the $^4F_{3/2}$-$^4I_{11/2}$ ($Y_3 \rightarrow R_2$) transition was measured. The peak absorption cross section, given in Eq. (4), is equal to the absorption coefficient divided by the lower-level population

$$\sigma_p(Y_3 \rightarrow R_2) = \alpha_p(Y_3 \rightarrow R_2)/N(Y_3) . \tag{4}$$

The absorption coefficient for the 10.13-cm-long Nd:LaLuGaG boule was measured to be 6.34×10^{-4} cm^{-1}. With the Nd^{3+} concentration of the Nd:LaLuGaG boule equal to 1.45×10^{20} Nd^{3+} ions/cm^3 (determined by x-ray fluorescence), and the partition function equal to 2.488 (data taken from Table IV), the population in the Y_3 Stark level at 2097 cm^{-1} is 2.32×10^{15} Nd^{3+}/cm^3 at 298 K. Substitution of these values into Eq. (4) yields a cross section of 2.73×10^{-19} cm^2. This value is 2.4 and 0.9 times smaller than the values for Nd:YAG and Nd:GSGG, respectively.[12]

F. Branching ratios and radiative lifetimes of Nd^{3+}:LaLuGaG

The branching ratios and the radiative lifetimes of the $^4F_{3/2}$-^4I_J ($J = \frac{9}{2}, \frac{11}{2}, \frac{13}{2}, \frac{15}{2}$) were determined in two independent ways. The first method is a direct application

of the Judd-Ofelt theory[13,14] and has been used by many authors.[15-17] Data analysis was performed similar to that of Krupke[17] and is briefly described below.

The integrated absorption coefficient, $\int k(\lambda)d\lambda$, emanating from the ground state $|(SL)J\rangle {}^4I_{9/2}$ manifold to excited $|(S'L')J'\rangle$ manifolds was measured for 11 absorption bands in Fig. 1. The integrated absorption coefficient in turn is related to the line strength S by Eq. (5):[1]

$$\int k(\lambda)d\lambda = \frac{8\pi^3 N_0 \bar{\lambda}e^2}{3ch(2J+1)} \left[\frac{(n^2+2)^2}{9n} \right] S , \tag{5}$$

where J is the total angular momentum quantum number of the initial level, $\bar{\lambda}$ is the mean wavelength that corresponds to the J-J' transition, n is the index of refraction, and N_0 is the Nd^{3+} concentration. Values for n were taken from Sellmeier's dispersion equation, Eq. (3), and N_0 was 1.45×10^{20} ions/cm^3. The Judd-Ofelt theory predicts that the line strength S may be written in the form

$$S([SL]J,[S'L']J')$$
$$= \sum_{t=2,4,6} \Omega_t |\langle 4f^n[SL]J\|U^{(t)}\|4f^n[S'L']J'\rangle|^2 , \tag{6}$$

where $\langle 4f^n[SL]J\|U^{(t)}\|4f^n[S'L']J'\rangle$ is a reduced-matrix element of the irreducible tensor operator of rank t, and Ω_t are the Judd-Ofelt parameters. The numerical values of the squares of the reduced-matrix elements for Nd^{3+} (aquo) ions for transitions from the ground state were taken from Carnall, Fields, and Rajnak.[18] When the absorption band was a superposition of lines assigned to several intermultiplet transitions, the matrix element was taken to be the sum of the corresponding squared matrix elements.[1] A least-squares fitting of S_{calc} to S_{meas} yields values for $\Omega_{2,4,6}$. Table V shows the measured and calculated line strengths for 11 absorption bands. The Judd-Ofelt parameters and the branching ratios are given in Table VI.

TABLE V. Measured and calculated line strengths of Nd^{3+} in LaLuGaG.

Russell-Saunders state $[S'L']J'$	Wavelength (nm)	Index of refraction n	Line strengths (10^{-20} cm^2) S_{meas}	S_{calc}
$^4F_{3/2}$	882	1.8738	0.424	0.749
$^4F_{5/2} + {}^2H_{9/2}$	807	1.8805	2.137	1.984
$^4F_{7/2} + {}^4S_{3/2}$	748	1.8874	1.741	1.842
$^4F_{9/2}$	683	1.8973	0.144	0.133
$^2H_{11/2}$	625	1.9092	0.014	0.034
$^4G_{5/2} + {}^2G_{7/2}$	587	1.9193	1.594	1.594
$^2K_{13/2} + {}^4G_{7/2} + {}^4G_{9/2}$	526	1.9410	0.886	0.898
$^2K_{15/2} + {}^2G_{9/2} + ({}^2D,{}^2P)_{3/2}$	479	1.9648	0.130	0.176
$^4G_{11/2}$	459	1.9778	0.084	0.016
$^2P_{1/2} + {}^2D_{5/2}$	433	1.9982	0.041	0.103
$^2P_{3/2} + {}^2D_{3/2} + {}^4D_{3/2} + {}^4D_{5/2}$	356	2.0988	0.980	0.789

TABLE VI. Experimental and theoretical Judd-Ofelt parameters and predicted branching ratios in Nd^{3+}:LaLuGaG.

Parameters	Experimental value	Theoretical value
	Judd-Ofelt	
Ω_2	0.84×10^{-20} cm^2	0.31×10^{-20} cm^2
Ω_4	2.64×10^{-20} cm^2	1.21×10^{-20} cm^2
Ω_6	2.61×10^{-20} cm^2	5.19×10^{-20} cm^2
	Radiative lifetime	
$^4F_{3/2}$	362 μs,[a] 295 μs[b]	286 μs
	Branching ratios	
$\beta(^4F_{3/2}\text{-}^4I_{9/2})$	43.6%	26.0%
$\beta(^4F_{3/2}\text{-}^4I_{11/2})$	47.2%	59.5%
$\beta(^4F_{3/2}\text{-}^4I_{13/2})$	8.8%	13.8%
$\beta(^4F_{3/2}\text{-}^4I_{15/2})$	0.4%	0.7%

[a]From Judd-Ofelt calculations.
[b]From fluorescence lifetime experiments.

The second method of determining the branching ratios and radiative lifetimes uses the point charge model. In these calculations, the Stark-level positions of Nd^{3+} given in Table IV were used along with the free-ion Russell-Saunders $[SL]J$ states with the free-ion Hamiltonian containing the Coulomb, spin-orbit, L^2, $G(G_2)$, and $G(R_7)$ interactions.[19] The free-ion parameters chosen, from Carnall, Fields, and Rajnak,[18] are $E^{(1)} = 4739.3$, $E^{(2)} = 23.999$, $E^{(3)} = 485.96$, $\zeta = 884.58$, $\alpha = 0.5611, \beta = -117.15$, and $\gamma = 1321.3$ (all in cm^{-1}). In the crystal-field analysis we assume a crystal electric field (CEF) of D_2 symmetry of the form

$$H_{\text{CEF}} = \sum_{ikq} B_{kq}^* C_{kq}(\hat{r}_i) , \quad (7)$$

where the B_{kq} are the crystal-field parameters and the $C_{kq}(\hat{r})$ are spherical tensors related to the spherical harmonics by

$$C_{kq}(\hat{r}_i) = \sqrt{4\pi/(2k+1)} Y_{kq}(\theta_i, \phi_i) . \quad (8)$$

The sum on i in Eq. (7) runs over the three electrons in the $4f^3$ configuration of Nd^{3+}, and the sum on k (k even) covers the range 2–6 with q even and in the range $-k \leq q \leq k$. Since we assume that the Nd^{3+} ions occupy the dodecahedral site with D_2 symmetry, the crystal-field parameters can be chosen real; thus there is a total of nine even-k B_{kq}. The procedure we use in the analysis of the experimental data is to obtain the free-ion wave functions using the free-ion parameters. We then use these free-ion wave functions to evaluate the energy levels in a crystal using the Hamiltonian given in Eq. (7). The crystal-field parameters B_{kq} are then determined by minimizing the squared difference of the calculated energies from the experimental energies. The centroids of each $[SL]J$ multiplet are allowed to vary freely during this fitting and are considered experimental data in the final analysis.

To obtain starting values of B_{kq} for our fitting of the experimental energy levels, we use point-charge lattice sum A_{kq}. The A_{kq} are related to the B_{kq} by[20]

$$B_{kq} = \rho_k A_{kq} , \quad (9)$$

where

$$\rho_k = \tau^{-k} \langle r^k \rangle_{\text{HF}} (1 - \sigma_k) . \quad (10)$$

τ is an ion-dependent radial expansion parameter,[20] $\langle r^k \rangle_{\text{HF}}$ are Hartree-Fock expectation values,[21] and σ_k are shielding factors.[22] Values of ρ_k for Ce^{3+} through Yb^{3+} are given by Morrison and Leavitt.[23] The values of A_{kq} were calculated by a point-charge lattice sum using the x-ray data of Table I. In performing the lattice sum, the material is assumed to be $La_3Lu_2Ga_3O_{12}$, and for the starting parameters the charges on the individual ions are assumed to be the valence charges $q_{La} = 3$, $q_{Lu} = 3$, $q_{Ga} = 3$, and $q_0 = -2$ (in units of the electron charge). Later A_{kq} were calculated using an effective charge on the oxygen site q_0 such that $q_{Ga} = -5 - 4q_0$ and varying q_0 to obtain the best fit of calculated B_{kq} to experimental B_{kq}. The resulting A_{kq} for even k were obtained from the lattice sums; the B_{kq} obtained by using Eq. (9) are given in column 3 of Table VII. These values of B_{kq} were used in the least-squares fitting as starting parameters.

The crystal-field parameters that gave the best fit to the experimental data are given in Table VII, as well as the point-charge B_{kq} computed using $q_0 = -1.64$ (the value of the oxygen charge that gave the best agreement to the experimental B_{kq}). In this fitting a number of experimental levels were discarded because attempts to fit these levels were unsuccessful. The odd-k A_{kq} (cm^{-1}/Å^k) using $q_0 = -1.64$ were calculated and are $A_{32} = 1520$, $A_{52} = -1500$, $A_{54} = 867$, $A_{72} = 54.2$, $A_{74} = 88.0$, and $A_{76} = -129$. (All odd-k A_{kq} are imaginary.)

The B_{kq} of Table VII along with the odd-k A_{kq} values were used to calculate the intensity of electric and magnetic dipole transitions for the rare-earth series. A detailed discussion of this calculation is given by Leavitt

TABLE VII. Experimental and calculated crystal-field parameters, B_{kq}. Note: Odd-k A_{kq} (cm^{-1}/Å^k) for $q_0 = -1.64$ are $A_{32}=1520$, $A_{52}=-1500$, $A_{54}=867$, $A_{72}=54.2$, $A_{74}=88.0$, and $A_{76}=-129$.

kq	Best-fit experimental $B_{kq}{}^a$ (cm^{-1})	Point charge $B_{kq}{}^b$ (cm^{-1})
20	879	843
22	206	338
40	−80.4	68.6
42	−1650	−2370
44	−782	−1087
60	−1345	−1485
62	−608	−732
64	629	736
66	−613	−614

^{a}Best-fit experimental B_{kq} for all data; rms$=5.658$ cm^{-1}.
^{b}Point charge B_{kq} using $q_0 = -1.64$; rms$=50.38$ cm^{-1}.

and Morrison.[24] The resulting Judd-Ofelt intensity parameters are given in Table VI for Nd^{3+} and the other rare earths in Table VIII.

G. Nd^{3+}:LaLuGaG fluorescence and lifetime measurements

The fluorescence spectrum of Nd^{3+}:LaLuGaG was recorded with a Spex F222 spectrometer. Figures 2 and 3 show the fluorescence spectrum in the region of the $^4F_{3/2}$-$^4I_{11/2}$ and $^4F_{3/2}$-$^4I_{9/2}$ transitions. The fluorescence lifetime and time-resolved, site-selection spectroscopy measurements were made using a nitrogen laser-pumped tunable dye laser with rhodamine 6G for the excitation source. This provided pulses of about 10 ns in duration and less than 0.04 nm half-width. The 4.3 at. % Nd^{3+} sample was mounted in a cryogenic refrigerator with temperature variable between 10 and 300 K. The fluorescence was analyzed by a 1-m monochromator, detected by a cooled RCA C31034 photomultiplier tube, processed by an EGG-PAR boxcar integrator triggered by the laser, and displayed on an x-y recorder.

The fluorescence lifetime of Nd^{3+} in LaLuGaG after

TABLE VIII. Calculated Judd-Ofelt (JO) intensity parameters Ω_k of rare-earth ions in the La site of La$_3$Lu$_2$Ga$_3$O$_{12}$.

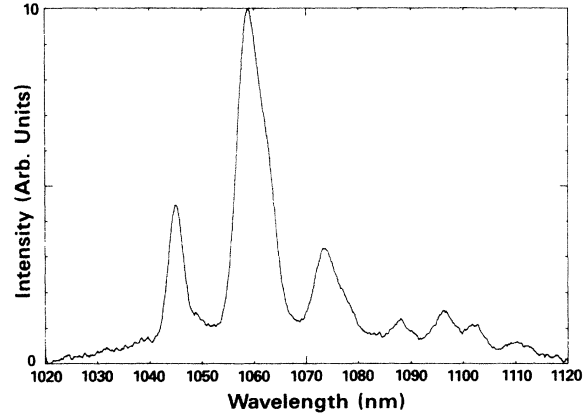| Ion	JO intensity parameters (10^{-20} cm^2) Ω_2	Ω_4	Ω_6
Ce	0.5872	3.734	22.17
Pr	0.3286	1.884	9.449
Nd	0.3167	1.206	5.186
Pm	0.1833	0.9318	3.986
Sm	0.1599	0.7902	3.300
Eu	0.1265	0.6060	2.333
Gd	0.0990	0.4588	1.610
Tb	0.1729	0.8314	3.913
Dy	0.1271	0.5830	2.428
Ho	0.1038	0.4601	1.772
Er	0.0995	0.4352	1.671
Tm	0.0968	0.4190	1.615
Yb	0.0817	0.3417	1.230

FIG. 2. Fluorescence of Nd^{3+}:LaLuGaG at room temperature in the region of the $^4F_{3/2}$-$^4I_{11/2}$.

lower power dye laser excitation varies from 290 μs at 11 K to 205 μs at room temperature, as shown in Fig. 4. The solid line in Fig. 4 represents the best fit to the data using an expression of the form

$$\tau_f^{-1} = \tau_r^{-1} + C\{\exp[\Delta E/(k_B T)] - 1\}^{-1}, \qquad (11)$$

where τ_f and τ_r are the fluorescence and radiative lifetimes, respectively. The last term describes the quenching of the lifetime due to radiationless processes involving the absorption of phonons of energy ΔE. C is a constant containing the matrix element for these transitions. The values obtained from fitting Eq. (11) to the experimental data are listed in Table IX. Several types of processes can lead to this type of lifetime quenching and will be discussed in Sec. II I.

H. Laser gain measurements

The laser-pumped, single-pass gain measurements using the frequency-doubled output of a mode-locked Nd-YAG laser as the pump source were performed at Oklahoma State University. This provided a 25-ps excitation pulse with a few millijoules of energy at 532 nm.
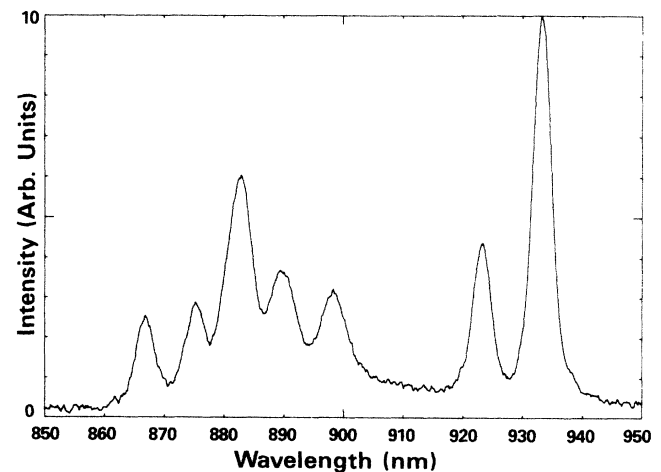

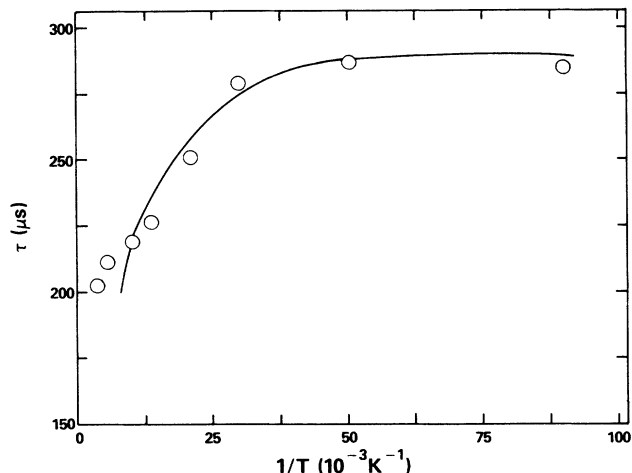FIG. 3. Fluorescence of Nd^{3+}:LaLuGaG at room temperature in the region of the $^4F_{3/2}$-$^4I_{9/2}$.

FIG. 4. Temperature dependence of the fluorescence lifetime of the $^4F_{3/2}$ metastable state of Nd^{3+}:LaLuGaG. (See text for explanation of the theoretical line.)

The probe beam was the collimated output of a xenon lamp passed through a 0.5-m monochromator. The change in the probe beam transmission through the sample under pumped conditions was monitored using a 0.25-m monochromator and photomultiplier tube with the output photographed on a storage scope. Multiphoton excitation studies were made using the same laser for excitation, and the fluorescence emission was monitored with a 0.25-m monochromator with an EGG-PAR silicon array detector and optical multichannel analyzer (OMA) combination. Fluorescence lifetimes under these excitation conditions were again measured with the boxcar integrator.

The attempt to observe single-pass gain was made with the probe beam tuned to the emission peak at 1059 nm while the pump beam at 532 nm was in resonance with one of the strong absorption transitions. Although these experimental conditions resulted in easily observable gain for several different types of Nd-doped crystal and glass

TABLE IX. Summary of results.

Parameter	Value
Fluorescence lifetime	
τ_f $^4F_{3/2}$ (10 K)	290 μs
τ_f $^4F_{3/2}$ (300 K)	205 μs
τ_f $^2P_{3/2}$ (300 K)	0.32 μs
τ_f $^2(F2)_{5/2}$ (300 K)	2.52 μs
Fluorescence rise time	
τ_{rt} $^2P_{3/2}$ (300 K)	317 ns
τ_{rt} $^2(F2)_{5/2}$ (300 K)	200 ns
Radiative lifetime	
τ_r $^4F_{3/2}$	295 μs
Energy transfer	
C	1538 μs
ΔE	30 cm^{-1}
α (100 K)	392 μs
ΔE_s	29 cm^{-1}

materials, no gain was observed for the 4.3 at. % Na^{3+}:LaLuGaG sample at room temperature. Since the optical quality (and thus the scattering losses per pass) was approximately the same for each of the samples investigated, the lack of optical gain indicates the presence of some type of loss process occurring for Nd^{3+} in the LaLuGaG host.

Direct lasing of two Nd:LaLuGaG samples was attempted at the Center for Night Vision and Electro-Optics. Two experiments were performed with different wavelengths of excitation and different pumping geometries. A laser diode array capable of producing 80 mJ per pulse at 20 Hz was used as a pump at 808 nm in a side-pump geometry. Typical outputs for Nd:YAG using this scheme are 25 mJ.[25] When a Nd:LaLuGaG sample was inserted in the resonator, no lasing was detected at 1059 nm. End-pumping of the same crystal was also attempted with a Coherent 699-29 ring dye laser producing 1.3 W with rhodamine 6G. Lasing was again not detected at 1059 nm. A focused dye laser beam at 595 nm produced an intense purple fluorescence at the focal point. This is indicative of two-photon absorption to higher lying levels, which prevents lasing in this material. This is consistent with the experimental results shown in Sec. II I.

I. Multiphoton excitation measurements

For low excitation powers, the fluorescence emission originates from the $^4F_{3/2}$ metastable state at wavelengths longer than 850 nm. After high-power picosecond pulse pumping, fluorescence emission extends throughout the visible region of the spectrum to about 800 nm, as shown in Fig. 5. This demonstrates the presence of multiphoton excitation processes and subsequent emission from higher energy metastable states. The spectral dynamics occurring under these pumping conditions have been studied for Nd^{3+} in YAG, $Y_3Ga_5O_{12}$ (YGG), and lithium silicate glass.[26,27] The transitions have been shown to originate on the $^2P_{3/2}$ and $^2F_{5/2}$ metastable states with lifetimes of about 0.3 and 3.0 μs, respectively. The fluorescence lines shown in Fig. 5 can be divided into one set having a lifetime of 0.3 μs and another set having a lifetime of 2.5 μs. In comparison to the previous results, we assign these transitions to lines originating on the $^2P_{3/2}$ and $^2(F2)_{5/2}$, respectively.

One important difference between the results obtained on Nd^{3+}:LaLuGaG and those obtained on other hosts is that strong emission from the $^4F_{3/2}$ level was observed for the other samples under these pumping conditions[26,27] but not for LaLuGaG. This implies that multiphoton excitation transitions lead to relaxation channels that bypass the $^4F_{3/2}$ metastable state and thus act as a loss mechanism for pumping the $^4F_{3/2}$-$^4I_{11/2}$ laser transition. The multiphoton processes in the other hosts have been shown to be sequential two-photon excitation processes (STEP's) involving a real intermediate state,[27] and we assume that the same mechanism is active in LaLuGaG. The effects of the STEP mechanism appear to be stronger in the LaLuGaG sample than in the other hosts. One important spectral difference that may account for this is
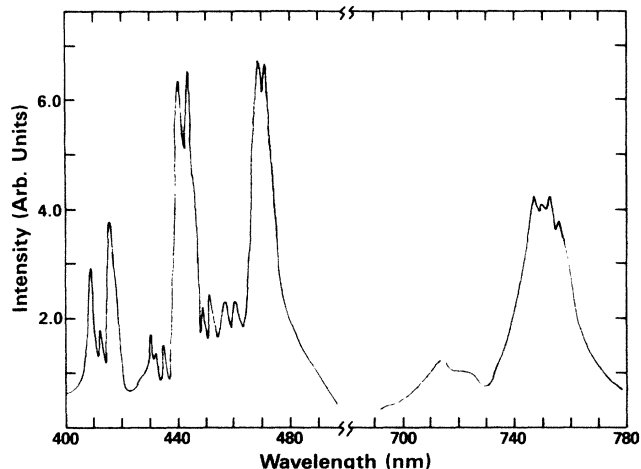
FIG. 5. Fluorescence of Nd^{3+}:LaLuGaG at room temperature after pumping at 532 nm with a 25-ps laser pulse.

that the 532-nm pump wavelength is almost exactly in resonance with an absorption transition in LaLuGaG, whereas for the other hosts investigated this wavelength is on the wing of the absorption band.

J. Energy transfer measurements

Dye laser, time-resolved spectroscopy techniques were used to investigate the characteristics of energy transfer between Nd^{3+} ions in nonequivalent crystal-field sites in the region from 560 to 600 nm. The fluorescence in the 880-nm spectral region was monitored in this investigation and is shown in Fig. 6 for two temperatures. At 11 K these transitions are associated with emission from the $^4F_{3/2}$ metastable state to the various Stark components of the $^4I_{9/2}$ ground-state manifold. At room temperature, emission from higher excited states is present and the transitions broaden because of both electron-phonon interactions and energy transfer to ions in spectrally inequivalent sites.
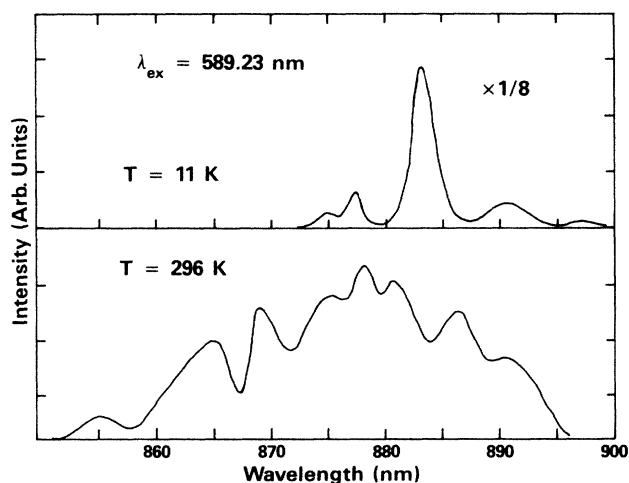
Microscopic strains produce slightly different crystal fields at the site of each Nd^{3+} ion in the lattice, resulting in inhomogeneous broadening of the spectral lines. In addition, Nd^{3+} ions occupying sites having significantly different crystal-field environments produce transitions that are easily resolvable in the optical spectra. Ions in a specific type of site can be selectively excited by tuning the dye laser into resonance with one of the absorption transitions associated with these ions. The results of doing this are shown in Fig. 7. As the excitation wavelength is tuned over 0.41 nm, the maximum emission of this transition shifts from peak a to peak b, indicating a change in the type of ion being excited. Note that the energy separation of the transitions originating from the ions in these two types of sites is $\Delta E_s = 29$ cm^{-1}.

In order to study the energy transfer between Nd^{3+} ions in these two major types of sites, the time evolution of the relative fluorescence intensities of peaks a and b was monitored as a function of time after the excitation pulse for both excitation wavelengths. These time-resolved measurements were carried out at several temperatures between 11 and 100 K, above which the thermal broadening of the lines prevented the spectral resolution necessary for accurate measurements. In this temperature range, no variation was observed in the ratios of the intensities of peaks a and b as a function of time. This indicates that energy transfer between Nd^{3+} ions in these two different types of sites is a very weak
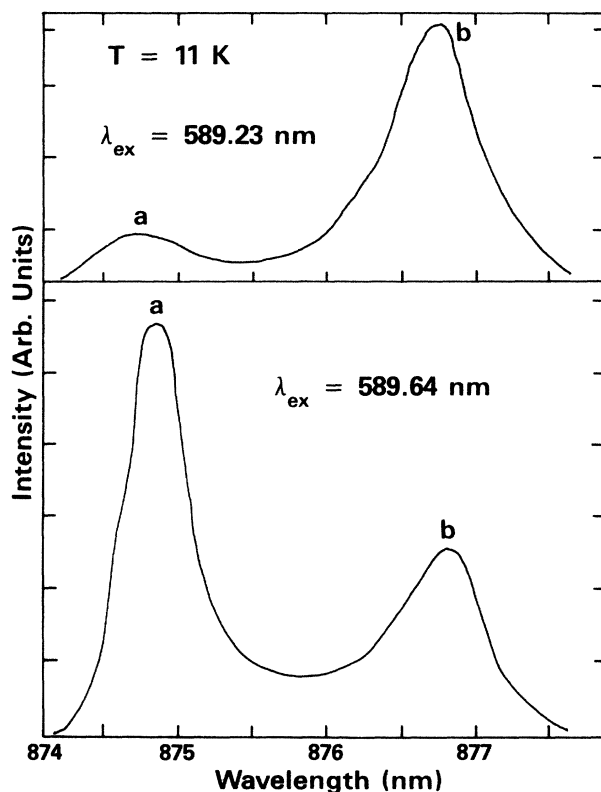

FIG. 6. Fluorescence of Nd^{3+}:LaLuGaG at two temperatures in the region of the $^4F_{3/2}$-$^4I_{9/2}$ transition after pumping near 589 nm with a 10-ns laser pulse.

FIG. 7. Fluorescence of Nd^{3+}:LaLuGaG at 11 K in the region of one of the $^4F_{3/2}$-$^4I_{9/2}$ transitions for two different excitation wavelengths.
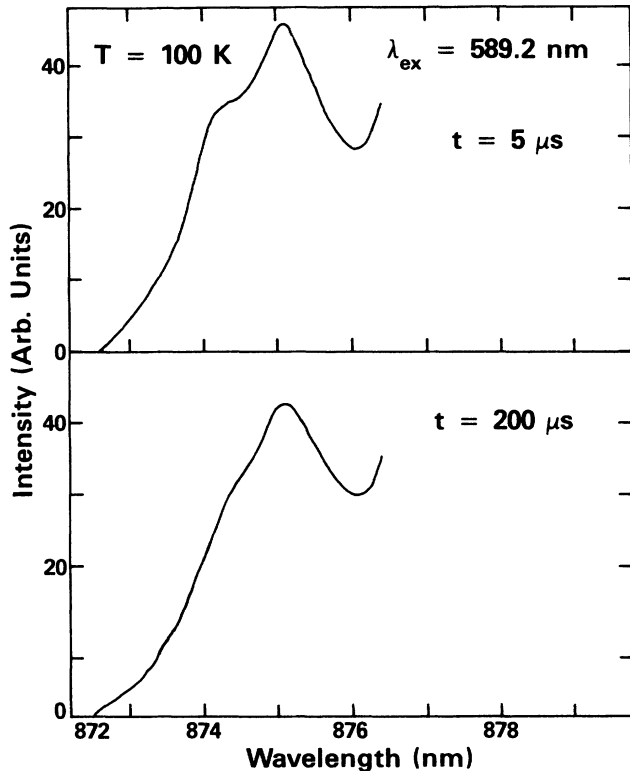
FIG. 8. Fluorescence of Nd^{3+}:LaLuGaG at 100 K in the 875 nm spectral region at two different times after the excitation pulse.

process. However, the similarity of the activation energy for thermal quenching of the fluorescence lifetime and the energy difference between peaks a and b may indicate that at higher temperatures energy transfer between ions in these two major types of sites does occur and results in the quenching of the decay time.

Even though energy transfer between ions in the two major types of sites is negligible at low temperatures, time-resolved spectroscopy measurements do reveal spectral energy transfer across an inhomogeneously broadened line. An example of this is shown in Fig. 8 where the shape of fluorescence transition a is shown for two times after the laser pulse at 100 K. A distinct high-energy shoulder appears on this line at short times and disappears at long times. This can be attributed to the presence of energy transfer between Nd^{3+} ions in type a sites with differences in transition energies due to local perturbations of their surrounding crystal fields. This type of energy transfer can be treated quantitatively in the formalism developed for analyzing spectral energy transfer in doped glasses.[28] In this model, the time evolution of the fluorescence intensity at frequency ω is expressed as

$$I(\omega,t)=a(t)I(\omega,0)+[1-a(t)]I(\omega,\infty) , \qquad (12)$$

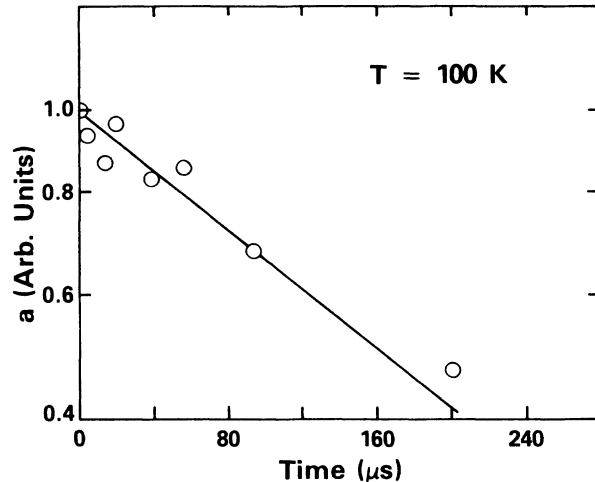where $a(t)$ is the function describing the energy transfer. This can be integrated to give

FIG. 9. Time dependence of the energy-transfer function $a(t)$ at 100 K obtained from Eq. (13) by monitoring the time evolution of the shape of the fluorescence band at 875 nm.

$$a(t)=\int_{\omega_1}^{\omega_2}[I(\omega,t)-I(\omega,\infty)]d\omega$$
$$\times\left[\int_{\omega_1}^{\omega_2}[I(\omega,0)-I(\omega,\infty)]d\omega\right]^{-1} . \qquad (13)$$

The results of this analysis at 100 K are plotted in Fig. 9. The energy transfer function decreases exponentially with time, having a characteristic time constant of $\alpha=392$ μs. The energy transfer parameters are summarized in Table IX.

III. SUMMARY AND CONCLUSIONS

The lifetime results summarized in Table IX indicate that Nd^{3+} ions in LaLuGaG have a quantum efficiency near 98%, which is significantly higher than that for Nd:YAG crystals with this doping concentration.[1] In addition, the rate of energy transfer between ions in the two major types of nonequivalent crystal-field sites is much smaller than in the YAG host.[29] Since the quantum efficiency of $^4F_{3/2}$ fluorescence in Nd^{3+}-doped materials is generally attributed to cross-relaxation processes between neighboring Nd^{3+} ions which can be enhanced by energy migration among the Nd^{3+} ions, these results are indicative of weak ion-ion interaction processes in the LaLuGaG host. This observation is consistent with the increased ion-ion separation in the LaLuGaG crystal.

The origin of the two major types of nonequivalent crystal-field sites in LaLuGaG has not been identified. However, in comparison with the results of previous site-selection spectroscopy investigations of mixed garnet crystals,[3,29] it is reasonable to assume that the different sites are associated with different lutetium environments around the Nd^{3+} ions. In the YAG host, the energy transfer between ions in the different types of sites has been attributed to a two-phonon assisted process with a real intermediate state.[26,27] This leads to an activation energy associated with the energy level splitting of the lowest two ground-state Stark components which is

significantly greater than the measured activation energy in the Nd^{3+}:LaLuGaG crystal. This implies the presence of different types of energy transfer mechanisms in the two types of hosts.

The point-charge calculation of the odd-fold crystal fields (k=odd A_{kq}) was used to calculate the Judd-Ofelt intensity parameters, Ω_k, for all the rare-earth experimental values. For Nd^{3+}:LaLuGaG the radiative lifetime of the $^4F_{3/2}$ level was calculated and compares favorably with experiment. The branching ratios from a line-to-line intensity calculation for the $^4F_{3/2}$ to ^4I_J manifold were determined. The agreement of the crystal-field calculations with the experimental data was excellent for the ^4I_J and ^4F_J multiplets as well as the $^4S_{3/2}$ and $^4G_{5/2}$ energy levels.

The ability to incorporate high concentrations of Nd^{3+} in the lattice without degrading the optical quality and maintaining a high level of quantum efficiency would make LaLuGaG an attractive host for a Nd^{3+} laser material. However, the inability to observe lasing under pumping conditions producing gain in other Nd-doped materials, due to the presence of strong multiphoton transitions in this host, reduces the potential of Nd^{3+}:LaLuGaG as a replacement for Nd^{3+}:YAG or Nd^{3+}:Cr^{3+}:GSGG as an efficient 1-μm laser.

*Permanent address: Division of Earth and Physical Sciences, The University of Texas at San Antonio, San Antonio, TX 78285.

[1] A. A. Kaminskii, Laser Crystals (Springer-Verlag, Berlin, 1981).

[2] M. Kokta and M. Grasso, J. Solid State Chem. 8, 357 (1973).

[3] L. A. Riseberg and W. C. Holton, J. Appl. Phys. 43, 1876 (1972); L. A. Riseberg, R. W. Brown, and W. C. Holton, Appl. Phys. Lett. 23, 127 (1973); L. A. Riseberg and W. C. Holton, Opt. Commun. 9, 298 (1973).

[4] Yu. K. Voron'ko and A. A. Sobol', Trudy Ordena Lenima Fizicheskogo Instituta Im. P. N. Lebedeva, 98:39 (1982).

[5] W. Koechner, Solid State Laser Engineering (Springer-Verlag, New York, 1976), Vol. 1, p. 35.

[6] G. Menser, Z. Kristallogr. 63, 157 (1926).

[7] J. D. Dunitz, X-Ray Analysis and the Structure of Organic Molecules (Cornell University Press, New York, 1979), pp. 183–222.

[8] C. F. Campana and T. H. Allik, Science Applications International Corporation, Report No. 164-450-043, 1988 (unpublished).

[9] Micromatter Co., Rt. 1, Eastsound, WA 98245.

[10] B. R. Pamplin, Crystal Growth (Pergamon, Oxford, 1980), Vol. 16, p. 289.

[11] W. L. Bond, J. Appl. Phys. 36, 1674 (1965).

[12] W. F. Krupke, M. D. Shinn, J. E. Marion, J. A. Caird, and S. E. Stokowski, J. Opt. Soc. Am. B 3, 102 (1986).

[13] B. R. Judd, Phys. Rev. 127, 750 (1962).

[14] G. S. Ofelt, J. Chem. Phys. 37, 511 (1962).

[15] M. J. Weber, T. E. Varitmos, and B. H. Matsinger, Phys. Rev. B 8, 47 (1973).

[16] W. F. Krupke, IEEE J. Quantum Electron. QE-10, 450 (1974).

[17] W. F. Krupke, IEEE J. Quantum Electron. QE-7, 153 (1971).

[18] W. T. Carnall, P. R. Fields, and K. Rajnak, J. Chem. Phys. 49, 4412 (1968); 49, 4424 (1968); 49, 4434 (1968); 49, 4444 (1968); 49, 4450 (1968).

[19] B. G. Wybourne, Spectroscopic Properties of Rare Earths (Wiley, New York, 1965).

[20] C. A. Morrison, N. Karayianis, and D. E. Wortman, Harry Diamond Laboratories, Report No. HDL-TR-1816, 1977; U.S. National Technical Information Service, Report No. A042447, 1977.

[21] A. J. Freeman and R. E. Watson, Phys. Rev. 127, 2058 (1962).

[22] P. Erdos and J. H. Kang, Phys. Rev. B 6, 3393 (1972).

[23] C. A. Morrison and R. P. Leavitt, J. Chem. Phys. 71, 2366 (1979).

[24] R. P. Leavitt and C. A. Morrison, J. Chem. Phys. 73, 749 (1980).

[25] D. Caffey (private communication).

[26] G. E. Venikouas, G. J. Quarles, J. P. King, and R. C. Powell, Phys. Rev. B 30, 2401 (1984).

[27] G. J. Quarles, G. E. Venikouas, and R. C. Powell, Phys. Rev. B 31, 6935 (1985).

[28] S. A. Brawer and M. J. Weber, Appl. Phys. Lett. 35, 31 (1979).

[29] L. D. Merkle and R. C. Powell, Phys. Rev. B 20, 75 (1979); M. Zokai, R. C. Powell, G. F. Imbusch, and B. DiBartolo, J. Appl. Phys. 50, 5930 (1979).